Spatial and temporal variability of free tropospheric freezing level in Patagonia

Nicolás García-Lee[1], Claudio Bravo[1], Álvaro Gónzales-Reyes[2,3,4,5], Piero Mardones[6]

[1]Glaciología y Cambio Climático, Centro de Estudios Científicos (CECs), Valdivia, 5090000, Chile.
[2]Instituto de Ciencias de la Tierra (ICT), Facultad de Ciencias, Universidad Austral de Chile, Valdivia 5090000, Chile.
[3]Laboratorio de Dendrocronología y Cambio Global, Universidad Austral de Chile, Valdivia, 5090000, Chile.
[4]Centro de Humedales Río Cruces (CEHUM), Universidad Austral de Chile, Valdivia, 5090000, Chile
[5]Centro de Investigación, Dinámica de Ecosistemas Marinos de Altas Latitudes (IDEAL), Universidad Austral de Chile, Valdivia, 5090000, Chile.
[6]Centro de Investigación en Ecosistemas de la Patagonia (CIEP), Coyhaique, 5950000, Chile.

Correspondence to: *Nicolás D. García Lee* (ngarcia@cecs.cl)

Abstract. The free tropospheric height of the 0°C isotherm (H0), commonly referred to as the freezing level, denotes the lowest altitude within a specific location's atmosphere where the air temperature reaches 0°C. This serves as an indicator for the transition between rain and snow, making it useful for monitoring and visualizing the altitude of freezing temperatures in the atmosphere. We study the spatial and temporal variability of H0 across Patagonia (41°-54°S) for the 1950-2021 period. Our results highlight the contrast around the Andes, manifested in lower/higher H0 on the western/eastern side, indicating the orographical influence on temperature vertical profiles on both sides of mountains. Our results indicate that the spatial mean value of the isotherm field in the region is 1691 meters above sea level (m.a.s.l). In terms of seasonal variability, H0 ranges from 585 m.a.s.l (winter) to 3480 m.a.s.l (summer). Moreover, the significant trends calculated over the period only show positive values in the area. This indicates an upward trend in the isotherm, averaging an increase of 8 to 61 meters per decade from 1959-2021, where the higher value is over northwestern Patagonia. Empirical orthogonal function (EOF) analysis was performed on isotherm anomalies. The first empirical orthogonal function (EOF) mode of H0 variability accounts for 84% of the total variance, depicting a monopole structure centered in the northwest area. This mode exhibits a positive correlation with the spatial average H0 anomalies field, the Southern Annular Mode (SAM), temperature at 850 hPa in the Drake Passage, and sea surface temperature off the western coast of Patagonia; underscoring the significant role of these factors in influencing the vertical temperature profile within the region.

1 Introduction

Patagonia, situated in the southern region of South America, is renowned for its distinct meteorological conditions and glaciers molded by its geographical features (Aravena & Luckman, 2009; Bravo et al., 2021; Masiokas et al., 2020; Sau-ter, 2020). Spanning approximately from 40°S to 55°S, the austral Andes reaching heights of around 1500 m a.s.l act as an

obstacle that hinders the progress of moist tropospheric air masses originating from prevailing westerly winds (Garreaud et al., 2009). The presence of this geographical barrier, along with the occurrence of baroclinic eddies, strong winds, and the

35 influence of the Pacific Ocean, generates a significant climatic distinction between the western and eastern areas of Patagonia, leading to a pronounced precipitation gradient (Garreaud et al., 2013). These effects are mainly driven by orographic or foehn effect, where a rise, expansion and cooling of the air on the windward side is observed. In leeward in-stead, precipitation is inhibited as descending air heats up and any lingering liquid water evaporates (Lenaerts et al., 2014; Roe, 2004; Siler et al., 2013). Consequently, the western slopes receive substantial precipitation ranging from 3000 to 7000

40 mm/year, fostering the growth of lush rainforests, rivers, and numerous glaciers. Conversely, the eastern slope ex-hibits a semi-arid steppe climate with a rain-shadow effect, receiving less than 500 mm/year of precipitation (Viale & Garreaud, 2014). The climate of Patagonia is strongly influenced by modes of variability, being the Southern Annular Mode (SAM) the primary driver of extratropical climate variability in the Southern Hemisphere. The SAM significantly affects the westerly flow, shaping the atmospheric circulation patterns in the region. It is characterized by an equivalent barotropic, zonally

45 symmetric structure that involves the exchange of mass between the mid and high latitudes (Garreaud et al., 2009). During its positive phase, the SAM strengthens and shifts the polar jet stream poleward. This intensifies the westerly flow, leading to notable changes in temperature and precipitation patterns across Patagonia. Conversely, during its negative phase, the SAM weakens and shifts the polar jet stream equatorward, impacting atmospheric circulation and influencing the region's climate. As a result, the variations in the SAM play a crucial role in modulating the westerly flow and have significant implications.

50 In the positive phase, higher temperatures, intensified westerly winds toward higher latitudes, and increased precipitation are observed below 40°S (Bravo et al., 2019; Fogt & Marshall, 2020). Conversely, the negative phase of the SAM produces contrasting effects, leading to wetter conditions in southern Patagonia (Carrasco-Escaff et al., 2023). Importantly, during the latter half of the 20th century, the SAM exhibited a positive trend, potentially influenced by anthropogenic factors (ozone depletion and increase of greenhouse gases), which could have implications for future climatic (Abram et al., 2014; Fogt &

55 Marshall, 2020). Carrasco-Escaff et al. 2023, elucidate another key atmospheric system in the region, called the "Drake Low," which exhibits anomalies in cyclonic circulation around the Drake Passage. These anomalies extend longitudinally from the Amundsen Sea to the northeastern part of the Antarctic Peninsula and latitudinally from the western Antarctic coast to the southernmost tip of South America (confined within the R1 area). The presence of the Drake Low results in an intensification of westerly winds, which notably affects the Patagonian region. This intricate system operates through a

60 thermodynamic mechanism, facilitated by a core of cold air, playing an active role in cooling the Patagonian region during the summer months. The study's findings provide valuable insights into the complex interplay between large-scale atmospheric dynamics and their direct influence on regional climate patterns. Revisiting the distinctive attributes of the region, the Northern and Southern Patagonian Icefields (NPI and SPI), which encompass the largest glacier area in Patagonia, playing an important role in the local and regional environment (Dussaillant J. et al., 2012). Recent research

65 underscores their significant contribution to the rise in sea levels compared to other ice masses in South America (Malz et al., 2018; Masiokas et al., 2020; Minowa et al., 2021), and the increasing loss of mass over the past few decades (Hugonnet

et al., 2021). And it is because of the sustained in atmospheric warming, that a profound impact on the mass balance of glaciers (Van der Geest & Van den Berg, 2021), especially in terms of the 0°C isotherm (Schauwecker et al., 2017). Because of changes in the distribution of this variable across territories, resulting in reduced snow accumulation, amplified melting,

70 and heightened flow rates during moderate or extreme precipitation events, such as atmospheric rivers. This, in turn, renders the region more susceptible to natural hazards, including an increased risk of floods (Somos-Valenzuela et al., 2020), landslides, and glacial lake outburst floods (Iribarren et al., 2015; Mardones & Garreaud, 2020). Nonetheless, the limited availability of data and analysis (particularly at the highest elevations) has hindered our comprehensive understanding of the fundamental mechanisms governing the interaction between these variables and the freezing level, especially the large-scale

75 climate processes operating on different timescales. As a result, there are still constraints on our knowledge in this domain.

The aim of this study is to assess and quantify the patterns and variations of isotherm 0°C in Patagonia. In the first section, we estimated the freezing level values based on ERA5 reanalysis data (climate grided product), which were subsequently validated with observed data from 4 radiosonde stations. Next, we used modeled data from 1950-2021 to analyze spatial patterns, seasonal and annual cycles, interannual variability, and trends in the area. The limitations of the model, spatial-

80 temporal distribution, large-scale drivers, and their implications are discussed.

2 Data and Methods

2.1 Study Area

Our research focuses on a vast expanse of Patagonia, delineated by a red rectangle in Figure 1a. This region spans latitudes

85 from 41° to 54°S and longitudes from 78° to 66°W, encompassing small fractions of both the Pacific and Atlantic Oceans. The selection of this domain was guided by the locations of radiosonde stations, specifically Puerto Montt (northwest), Comodoro Rivadavia (northeast), Río Gallegos (southeast), and Punta Arenas (south). Despite potential limitations posed to the west by Puerto Montt (as border domain point), we extended the area towards the west (78°W) to include a significant portion of western Patagonia and the eastern Pacific coast. Moreover, this longitudinal range encompasses the austral Andes

90 (AA) and the expansive glaciers of the Northern and Southern Patagonia Ice Field (NPI and SPI, respectively).
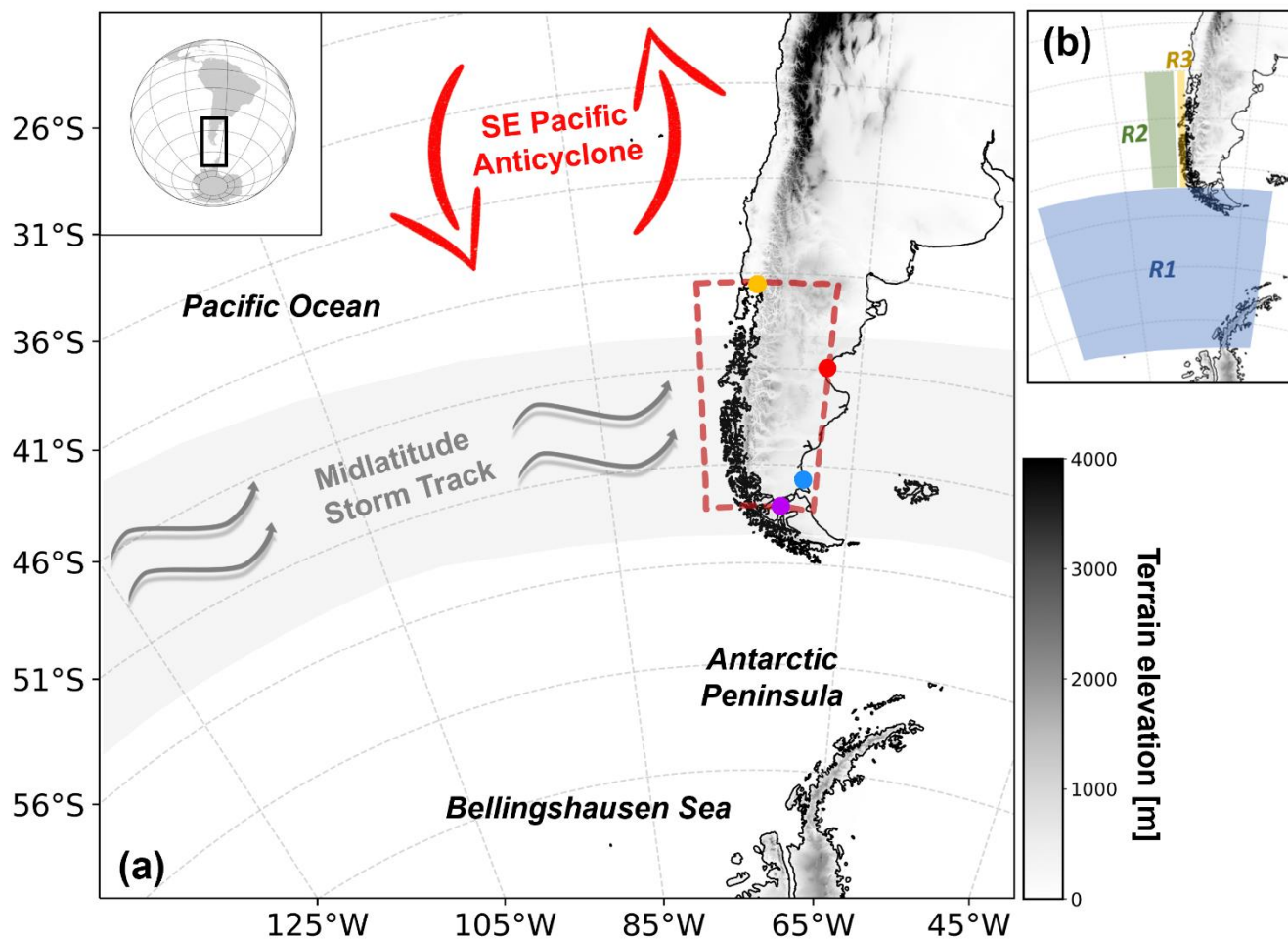
Figure 1: a) Topographic map of South America highlighting key features in the Patagonia region. Terrain elevation (m a.s.l) acquired from ETOPO1 model with 1 arcmin resolution. The red rectangle indicates the study region of Patagonia. The dots indicate the locations of the radiosonde stations of Puerto Montt (orange), Comodoro Rivadavia (red), Río Gallegos (blue), and Punta Arenas (purple). b) Colored areas represent the regions used for the construction of custom climate indices.

2.2 Assesment of isotherm at 0°C

To estimate the free tropospheric values of the 0°C isotherm, two sets of data were used. The first one corresponds to ERA5 data (Hersbach et al., 2020). This reanalysis comprises a latitude-longitude grid with a spatial resolution of 0.25°x0.25°, encompassing 37 pressure levels. For our analysis, we utilize the hourly data spanning from 1950 to 2021. Then, we extract vertical profiles of air temperature and geopotential height, spanning levels from the surface up to 400 hPa. Each profile is analyzed to identify the temperature transition above and below 0°C. H0 is determined by utilizing linear interpolation between the geopotential heights corresponding to the transition levels. If multiple elevations of zero degree are found, for

4

105   instance, from temperature inversions, the lowest value is assigned to H0. Additionally, if no zero crossing levels are found, the corresponding value is flagged as missing. It should be noted that under this methodology, the height of H0 in the free troposphere, when intersecting the topography, does not have a real physical interpretation. To obtain a representative value per day, we calculate the daily average of H0 using five values (00, 06, 12, 18, 00 UTC). This approach ensures that we capture the diurnal variability and provide a comprehensive picture of the freezing level throughout the day. We utilized a

110   second dataset comprising observations from radiosonde stations. We applied the proposed methodology to estimate H0 values, allowing us to validate the freezing level values obtained from ERA5 at specific locations. These observed values were obtained from the Integrated Global Radiosonde Archive product (Durre et al., 2018). With this data, we implemented an additional criterion, specifically utilizing vertical profiles that included a minimum of 3 data points. Profiles with inadequate data were excluded from the analysis. Fourth locations with comparable recording periods were selected for

115   analysis: Puerto Montt, Comodoro Rivadavia, Río Gallegos and Punta Arenas. The selection criteria for these locations were established to include only those with a minimum of a decade's worth of data, while excluding other locations that do not meet this criterion. We compared the grid's closest point to the observation points and only 12Z data was used to assess the agreement between them. Only this hour was selected since it has a greater number of observations in the records. The outcomes of this process are summarized in Table 1, where pearson correlation, root mean square error (RMSE), standard

120   deviation and average was estimated in selected periods for each location.

2.3 Indices and Trends

To analyze large-scale patterns associated with H0, we followed the methodology of the NOAA Climate Prediction Center (https://www.cpc.ncep.noaa.gov/products/precip/CWlink/daily_ao_index/history/method.shtml, last access: 10 January 2024.) to construct the SAM index. This index is derived by projecting 700 hPa geopotential height anomalies onto the

125   loading pattern of the SAM, which is defined as the leading empirical orthogonal function (EOF 1) of monthly mean at the 700 hPa geopotential height anomalies from 20°S poleward during the period 1959-2021. Anomalies are computed relative to the corresponding month's mean over the same period. To ensure equal area weighting in the covariance matrix, the gridded data is weighted by the square root of the cosine of latitude. Besides, we performed spatial averaging of monthly ERA5 values for specific areas and variables, following the methodology outlined by Carrasco-Escaff et al. (2023). In Figure

130   1b, the R1 box represented the geopotential height at 300 hPa and air temperature at 850 hPa near the Drake Passage (68-53°S and 100-60°W). The R2 box represented the southeast Pacific SST adjacent to central Patagonia (52.5-41°S and 80-76°W). Lastly, the R3 box represented the zonal wind at 850 hPa impacting central Patagonia (52.5-41°S and 75.5-74.5°W). These time series were labeled as Z300-R1, T850-R1, SST-R2, and U850-R3, respectively. Our objective is to comprehend the similarities and influences that these regions and variables may exert on the temperature profile within the area. Trend

135   values of H0 are estimated, which are derived from the Seasonal Mann-Kendall test and Theil-Sen estimator (Wilks, 2019).

5

A trend was considered statistically significant if the p-value < 0.05. A summarized scheme of the methodology implemented is presented in Figure 2.
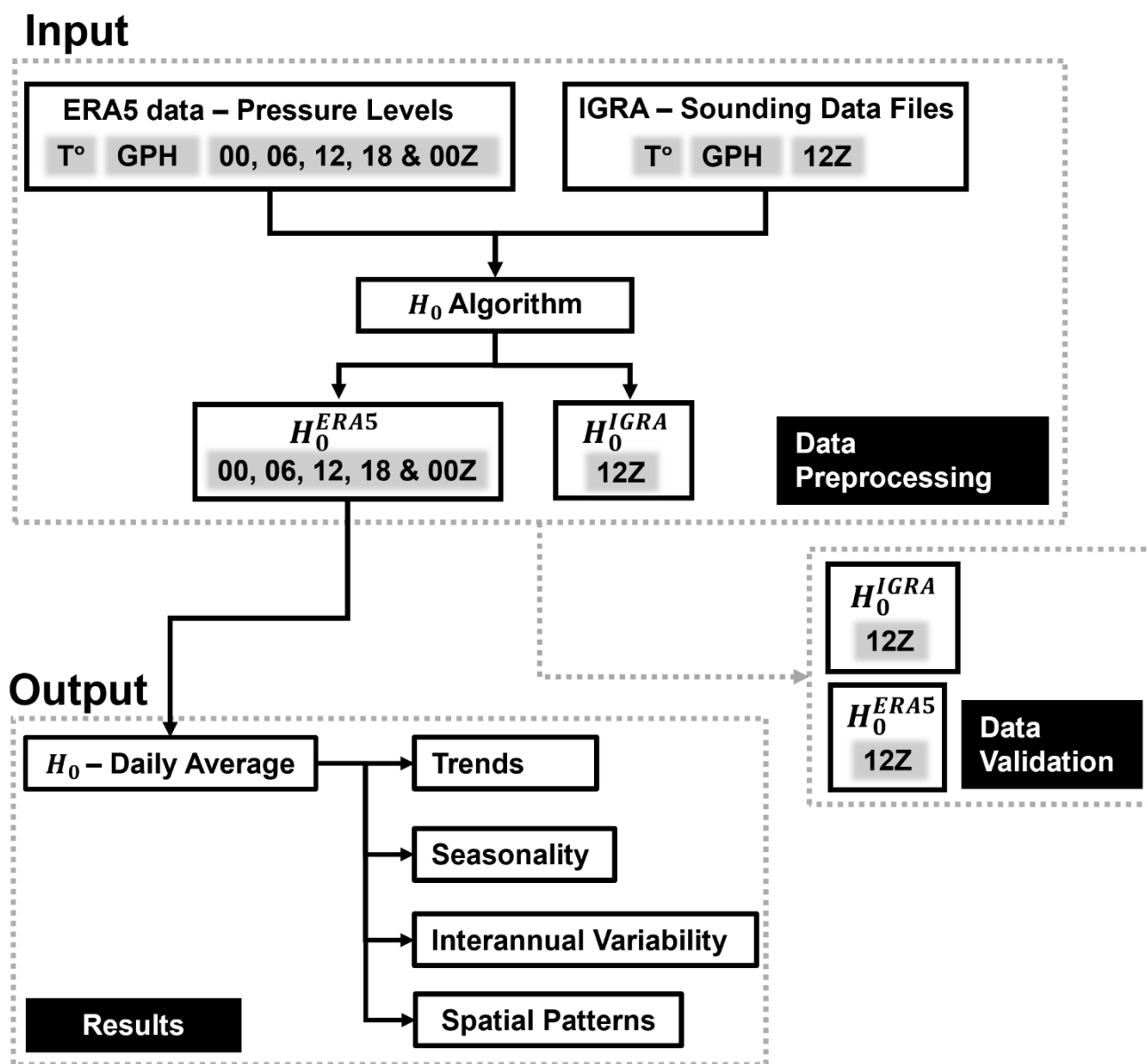

Figure 2: The data processing workflow for H0 between 1950 and 2021. Two distinct sets of input data were utilized: one comprising model data and the other containing radiosonde observations. The isotherm 0°C values were derived from these datasets, and a validation process was employed. Daily values were computed based on the model data.

3 Results

3.1 Validation

145 The statistical analysis between pairs of time series is presented in Table 1 and Figure 3, with hypothesis testing conducted at a significance level of 5% (*, p-value < 0.05). The results unveil significant relationships among the variables under investigation. Notably, the freezing level in Puerto Montt, Comodoro Rivadavia, Río Gallegos and Punta Arenas demonstrates a consistently strong positive correlation throughout the entire period (r = 0.97*, 0.96*, 0.8*, 0.94*, respectively).

150

In addition to reproducing the observed isotherm, the simulated isotherm also effectively captures the southern thermal gradient present within the study area. This pattern becomes apparent when examining the decreasing average heights of the modeled isotherms from Puerto Montt (2278±980 m a.s.l) to Punta Arenas (1176±655 m a.s.l). The noticeable disparity between the averaged isotherms for the northern and southern points of the study area further reinforces this observation.

155

Table1. Data and statistics of validation process between daily values of H_0^{IGRA} and H_0^{ERA5}. First columns indicate latitude (Lat.), longitude (Lon.), period, and number of data available (n_{obs}). Others columns depicted statistics as Pearson correlation (r*, values that are statistically significant at a p-value < 0.05), mean values $\overline{H}_0$, standard deviation (σ_0), mean bias error (MBE) and root mean-square error (RMSE).											
	Lat.	Lon.	Period	n_{obs}	r*	$\overline{H}_0^{IGRA}$	$\overline{H}_0^{ERA5}$	MBE	σ_0^{IGRA}	σ_0^{ERA5}	RMSE
Puerto Montt	-41.435	-73.098	1957-2021	21251	0.97	2314	2278	-36	961	980	252
Comodoro Rivadavia	-45.783	-67.500	1958-2021	17157	0.96	2100	2069	-30	864	869	240
Río Gallegos	-51.633	-69.217	1967-1977	2194	0.8	1487	1380	-107	714	633	445
Punta Arenas	-53.003	-70.845	1975-2021	11494	0.94	1287	1176	-111	655	655	251

On the other hand, the mean bias error (MBE) between modeled and observed values is negative at each comparison point, indicating that the modeled isotherm underestimates the observed one. The smaller MBE were estimated in the northern

160 zone, reaching an absolute minimum of 30 meters in Comodoro Rivadavia, followed by Puerto Montt with 36 meters. The larger biases were obtained for the southernmost zone, reaching an absolute maximum of 111 meters in Punta Arenas, closely followed by Río Gallegos at 107 meters. The calculated standard deviation for each pair of points was remarkably similar. The root mean square error for the longer series (at least 4 decades) ranges from 239-252 m a.s.l. For Río Gallegos, which has the smallest number of observations (~1 decade), the root mean square error increases to 445 m a.s.l. Despite this

165   increase, the average value of the data is not exceeded in any case by the RMSE; which indicates, the uncertainty is contained in the means of the data.
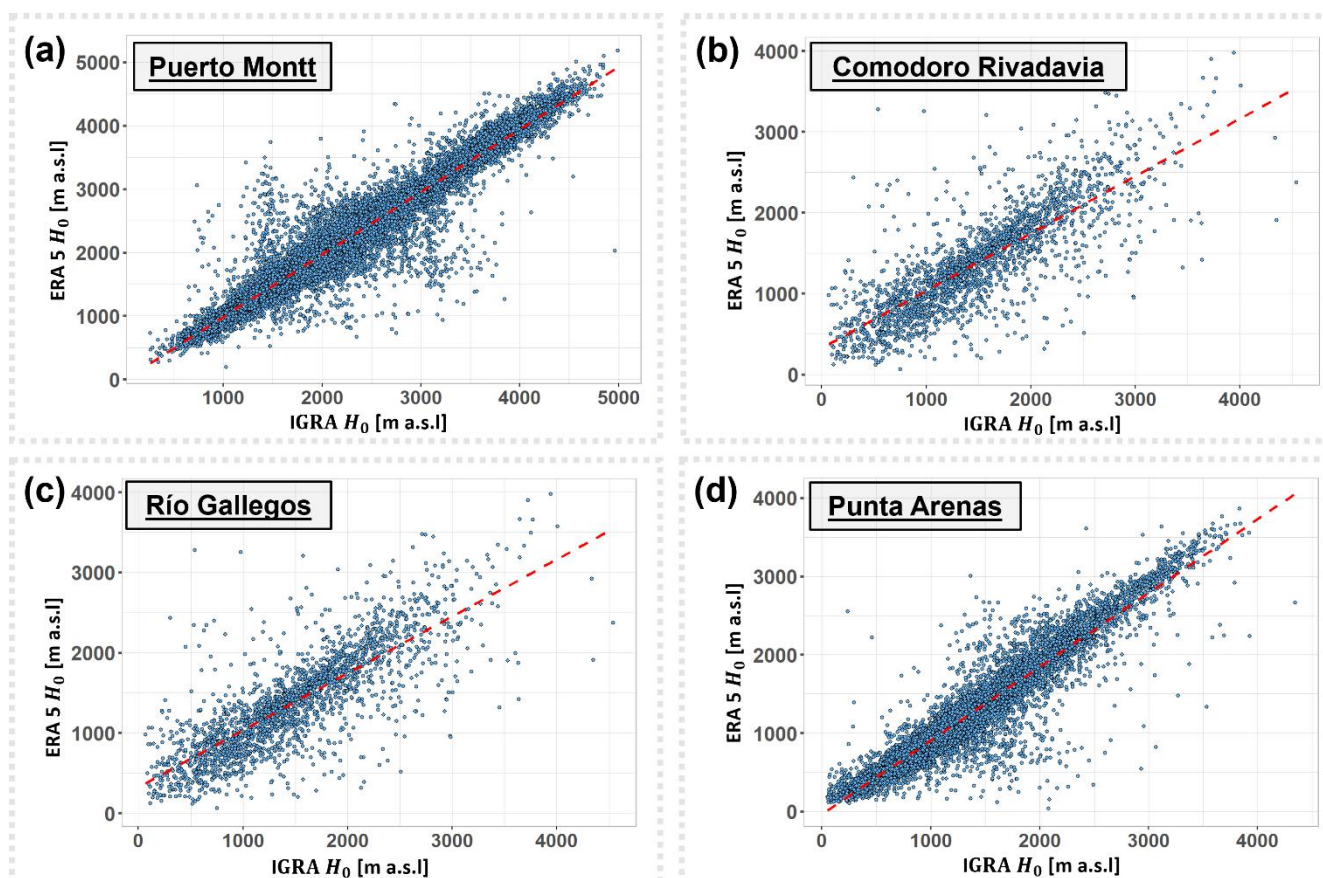

Figure 3: Scatterplots from Puerto Montt (a), Comodoro Rivadavia (b), Río Gallegos (c) and Punta Arenas (d). The reference data corresponds to the H0 observed (IGRA) and H0 modeled (ERA5) from the closest grid point in the ERA5 reanalysis. The red dotted line in scatterplots shows the 1:1 line.

3.2 Spatial patterns of H_0

175   The annual average of the H_0 field in the zone reveals a north-to-south variation, with higher height in the northern region and lower height in the southern region (Figure 4). The meridional profile shows a gradual decrease, intersecting with the topography between 47°-51°S. The interquartile range in this profile (IQR) indicates average fluctuations of around 257 m a.s.l, capture the extent of variations within the highest levels of the topography.

180 On the other hand, the zonal profile exhibits a more abrupt change in H_0 between 70°-74°W, coinciding with the presence of the highest peaks of the southern Andes. The zone exhibits a wide IQR of 695 m a.s.l, indicating significant variability in the H_0. This range encompasses the freezing level's proximity close to the lowest topography on the western side of the area. Conversely, in the eastern region, the range approaches H_0 only at the highest elevations on the eastern side. Spatially, the field representing the higher isotherms deepens further south from the eastern side. The western side shows that the field of

185 lower heights expands further north. Notably, this difference occurs around AA, which on average can be located around 72°W.
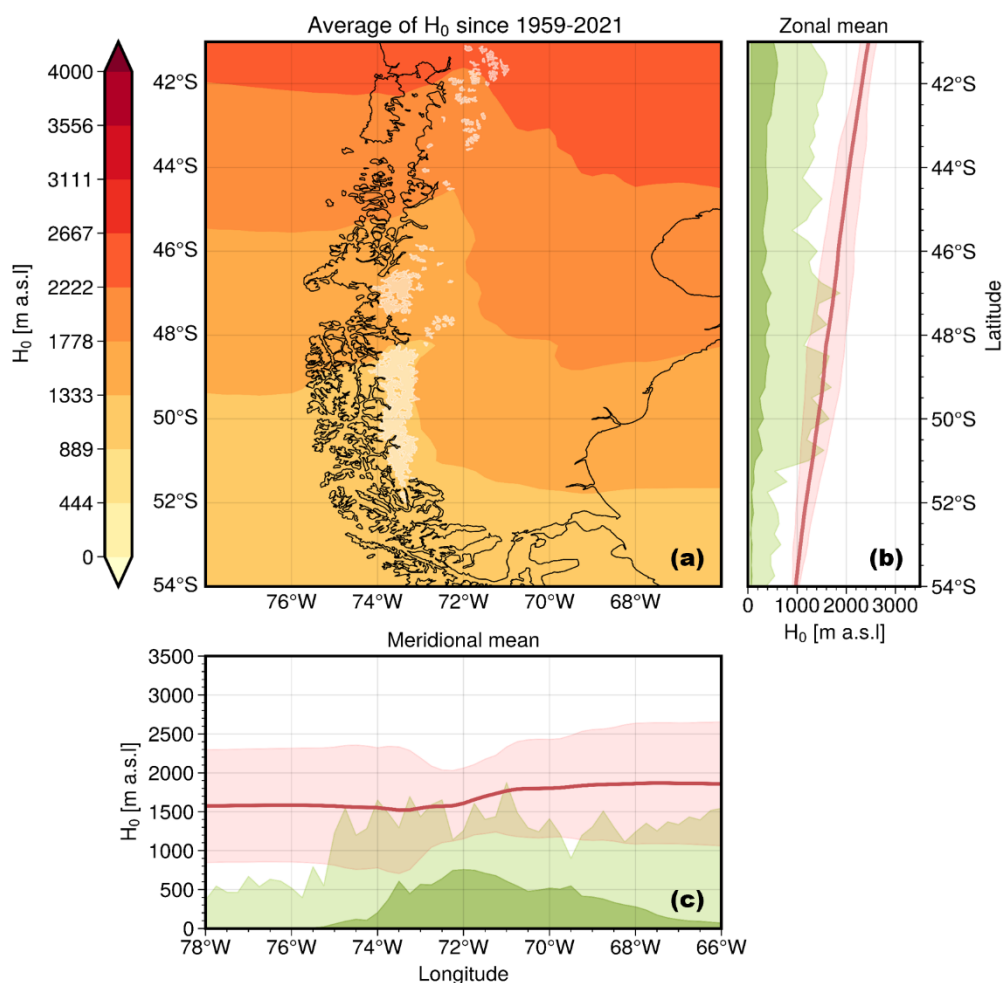

Figure 4: Spatial distribution of the annual average of H0 (a). Lighter areas depict a lower altitude of H0, while red areas indicate higher values. The white contours delineate the extent of ice coverage in the region. Each distribution is accompanied by a
190 **meridional profile (b) and a zonal profile (c), showcasing the spatially averaged H0 values. The red shaded area in these profiles represents the interquartile range (IQR). The green contours illustrate topographic profiles corresponding to the 2.5th percentile (dark green) and 97.5th percentile (light green).**

195   Consequently, we used this meridian as a reference of transitional boundary in the southern Andes (Figure 4), demarcating a middle ground where various regional geographical features converge. In doing so, we define western Patagonia as the region situated to the west of the 72°W meridian, while eastern Patagonia lies to its east. To illustrate the difference between these sides we used a histogram which expose the distribution of H_0 values spanning from 1951 to 2021, encompassing the entirety of the Patagonia region, as well as the western and eastern slopes. The daily freezing level values in the whole region

200   follow a distribution skewed to the right. The calculated average and median values stand at 1691 and 1519 m a.s.l, respectively. Notably, the upper extreme values (95th percentile) ascend to 3424 m a.s.l, while the lower extreme values (5th percentile) hover around 488 m a.s.l.

    There is a clear contrast between western and eastern Patagonia in terms of the altitude of H_0. Western Patagonia has a lower

205   altitude, as indicated by higher frequency of lower H_0 values with a mean and median which reach 1568 and 1347 m a.s.l, respectively. On the other hand, eastern Patagonia has higher frequency of higher values, with a mean and median of 1818 and 1708 m a.s.l, respectively. The difference between the two regions differs by approximately 251 (mean) to 362 m a.s.l (median) for the entire period.
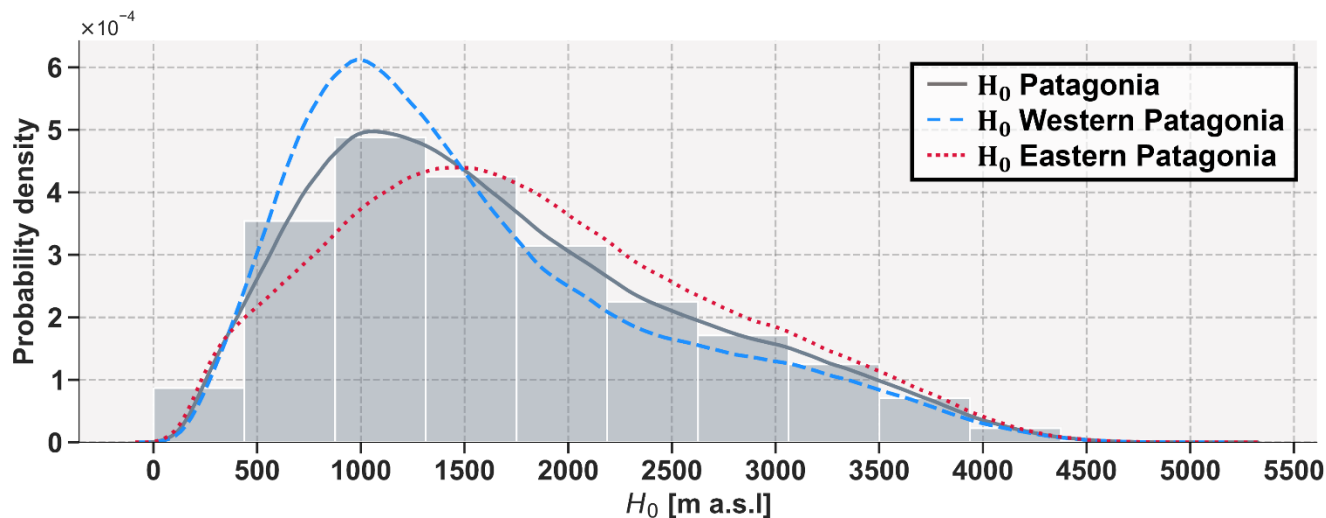
210

Figure 5: Histogram of daily simulated 0°C isotherm in Patagonia. The gray bars represent the daily values of H0 obtained from the spatial average across the entire study area from 1959 to 2021. The curves, on the other hand, indicate the fit of the kernel density estimation for the entire region (gray), Western Patagonia (blue), and Eastern Patagonia (red).

215

3.3 Seasonal cycle of H_0

The average variations of H_0 from north to south exhibit a marked seasonality (Figure 6). During the summer months, a distribution with higher heights is observed, reaching peak values in the mid-summer (January-February) over the region. From March, there is a sustained decrease in H_0, reaching its lowest point during winter (July-August). The estimated mean

220 amplitude indicates a range that fluctuates between 3480 to 585 m a.s.l (the highest absolute average in summer and winter). The average annual difference between the northernmost and southernmost zone of our study area is 1511 m a.s.l.
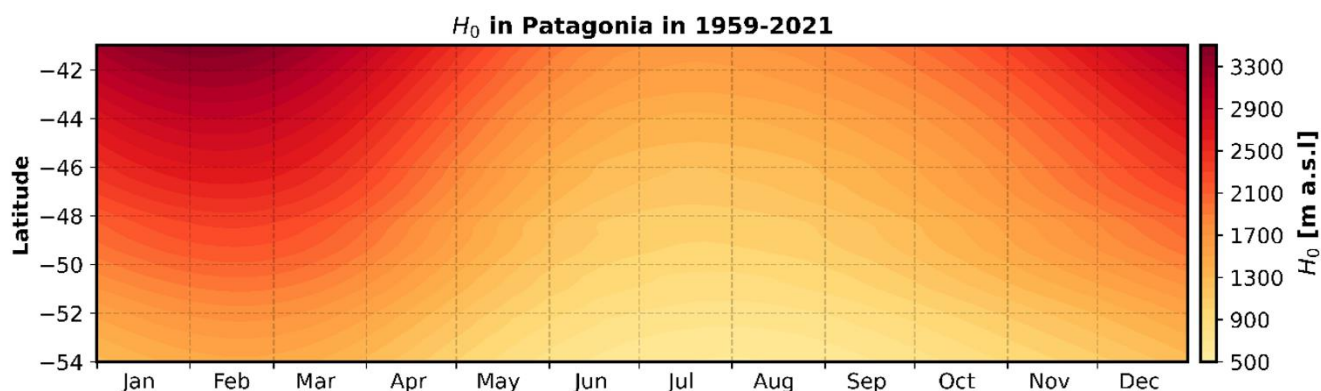

Figure 6: Latitudinal profile of daily climatology of H0 in Patagonia from 1959 to 2021.

225

A detailed examination of the seasonal averages provides further insights into the characteristics of the 0°C isotherm altitude in Patagonia (Figure 7). During summers, the average height of the isotherm is situated at 2236 m a.s.l, while the spatial distribution indicates how the longitudinal bands change concerning the east-west side of the AA (72°W). The meridional profile of the isotherm, along with its IQR, indicates that during this season, the freezing level altitude varies from 3383

230 (northern area) to 1188 (southern area) m a.s.l. This implies that the lowest isotherms during this period slightly reach the highest summits of the topography around 49.5-51°S. The zonal profile confirms that the longitudinal gradient intensifies around the Andes, with values ranging from 3383 (eastern area) to 931 m a.s.l (western area) along the profile. Additionally, the lower range of the isotherm allows for interception with the high AA topography, around at 72.5-75°W.

235 In autumn, the decrease in the freezing level altitude is evident. During this season, the average isotherm drops to 1891 m a.s.l, while the respective variations in the meridional and zonal profiles are smaller than summer, ranging from 2848-1066 and 2858-841 m a.s.l, respectively.

During the winter months, the lowest values of the field are recorded, where not only was an average 0°C isotherm estimated

240 at 1169 m a.s.l., but the variability of events is also contained within a narrower range spanning from 1799-591 (meridional

11

range) and 1931-447 m a.s.l (zonal range). These conditions allow the 0°C isotherm to intercept a significant portion of the higher and even lower terrain, especially around 73.5°W, as indicated by the zonal profile.

Notably, during the spring months, an average isotherm of 1477 m a.s.l was estimated, being the second lowest freezing level value after winter. For these months, an increase in the amplitude of the meridional and zonal isotherm ranges was already evident, with values ranging from 2449-701 and 2440-596 m a.s.l, respectively. However, despite the greater variability observed in the freezing level, the interception of the isotherm field with a significant portion of the higher terrain persists, particularly on the western slope of the Andes.

It is worth highlighting that the seasonal variations in Patagonia maintain and modulate the characteristic meridional and zonal gradient of the region, causing the estimated isotherm to fluctuate in a way that preserves its general spatial structure.
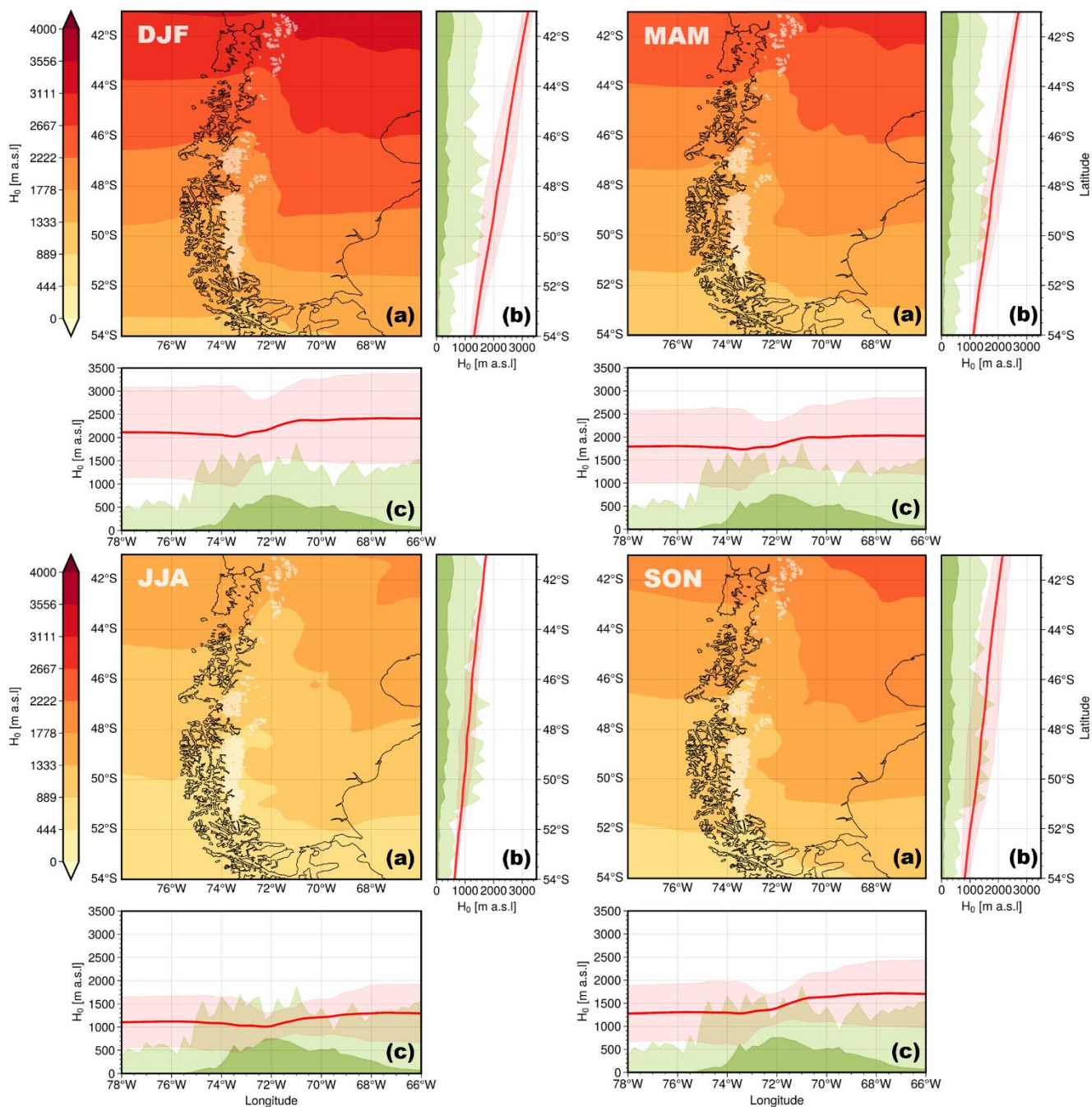
Figure 7: Spatial distribution of the seasonal averages of H0 (a). Lighter areas depict a lower altitude of the isotherm, while red
255 **areas indicate higher values. The white contours delineate the extent of ice coverage in the region. Each seasonal distribution is accompanied by a meridional profile (b) and a zonal profile (c), showcasing the spatially averaged H0 values. The red shaded area in these profiles represents the interquartile range. The green contours illustrate topographic profiles corresponding to the 2.5th percentile (dark green) and 97.5th percentile (light green).**

3.4 Large-scale control over H_0 variability

To investigate the large-scale influence on the freezing level in Patagonia, we conducted an Empirical Orthogonal Function (EOF) analysis on annual data of H_0 anomalies, following the methodology outlined in section 2.3. By applying North's rule of thumb (North et al., 1982), we selected the principal components of the first three main modes, which collectively account for 96% of the interannual variability (Figure S2). The spatial and temporal patterns of each mode are depicted in Figure 8. We additionally calculate correlations between these modes and the corresponding time series of diverse indices (SAM, NIÑO 1+2, NIÑO 3.4, R1-Z300, R1-T850, R2-SST, and R3-U850) at annual scales (see Figure 9). Regarding the SAM index, the resulting time series, represented by the first Principal Component (PC1), is normalized using the standard deviation of the monthly index based on the 1979-2000 base period (Figure S1).

Spatial patterns are shown through the regression between the principal component time series and the spatial distribution of the time-varying freezing level anomalies. The leading mode showcases a consistent EOF as it represents approximately 84% of the freezing level interannual variance. A remarkable concentration of positive H_0 anomalies (monopole) is observed, spreading from the northwest region of Patagonia (Figure 8a). Despite a reduction in magnitude, the core extension still encompasses several glaciers in the area, particularly in the northern region of NPI and along the northwest coasts, approximately between 44-46°S. Moving beyond these regions towards the northeast and poleward directions, the magnitude of anomalies diminishes gradually, but they consistently maintain a positive value.
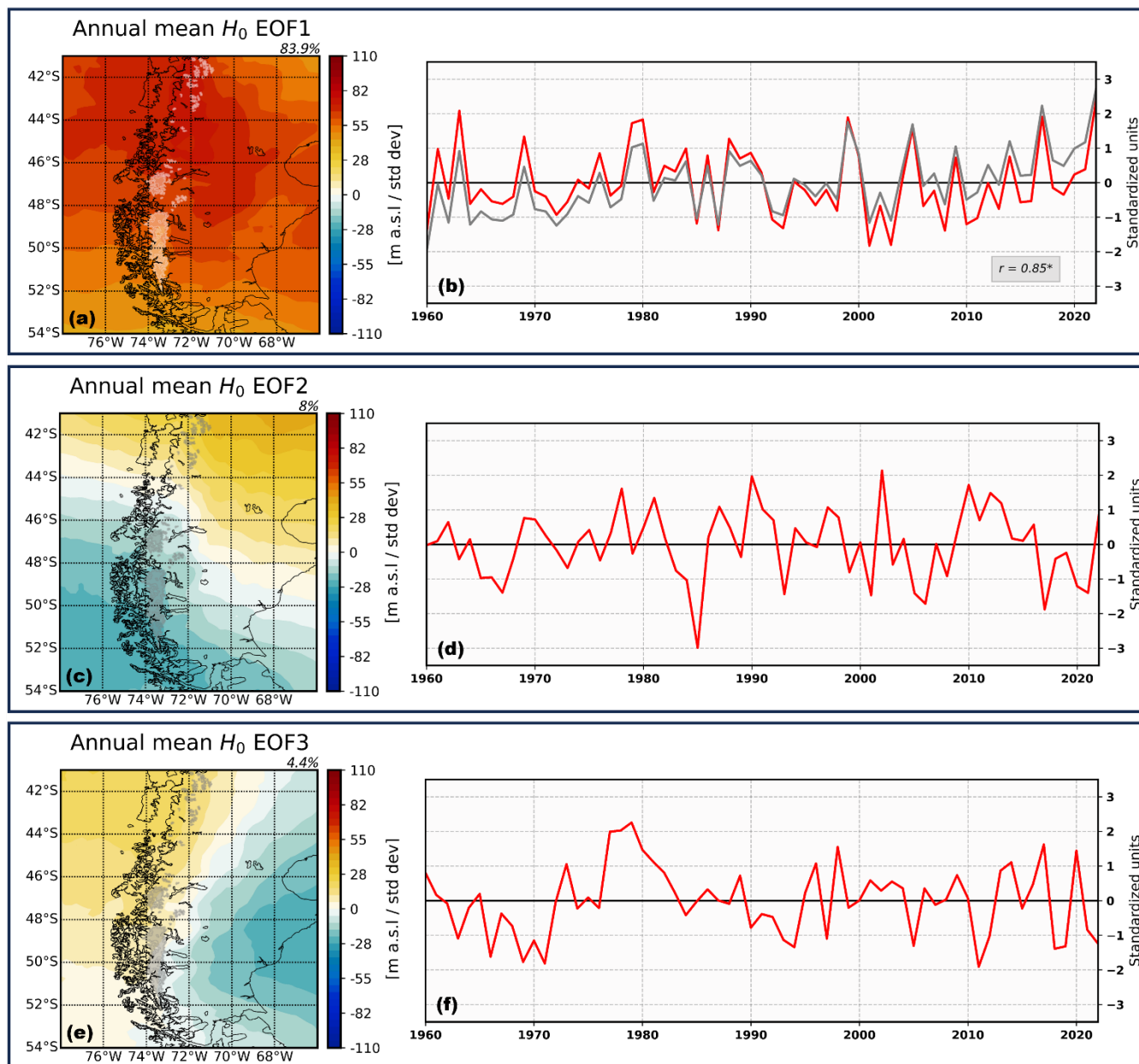
Figure 8: First three leading modes of variability extracted through an Empirical Orthogonal Function (EOF) analysis conducted on the annual freezing level field of Patagonia spanning from 1959 to 2021. (a, c & e) The resulting patterns are presented as regression maps, illustrating the relationship between the leading Principal Component (PC) time series and the spatial distribution of the time-varying height anomalies. Additionally, the temporal pattern is illustrated by the first Principal Component (red line), scaled to unit variance (divided by the square root of its eigenvalue), while the grey line portrays the standardized anomalies of the spatial average of the annual freezing level field across Patagonia (b, d & f). The box indicates Pearson's correlation between these two patterns. We continue the analysis for the second and third modes of variability (c-d and e-f, respectively). However, these modes show low correlation values with the freezing level anomalies, and thus, the focus is shifted away from freezing level anomalies in these cases. The white (a) and gray (c & e) contours delineate the extent of ice coverage in the region.

290

Regarding the temporal pattern, the PC1 exhibits strong alignment with the H_0 anomaly time series in terms of interannual variability (r=0.85*). These findings indicate that the large-scale climatic influences on variations are well-represented by the principal component analysis, providing valuable insights into interannual patterns of H_0 anomalies. Contrariwise, the second and third components do not show a significant relationship with H_0 anomalies ($|r| < 0.1$).

295

Therefore, years with H_0 above the average are characterized by a positive phase of SAM, alongside the presence of anomalous high temperatures around the Drake low and the sea surface temperature of Patagonia's west coasts. The positive phase of SAM is associated with subsidence and adiabatic heating on the equatorward side of the polar jet, leading to anomalies in precipitation and surface temperature, especially south of 40°S. Consequently, northern Patagonia experiences drier than average conditions, while southern Patagonia exhibits moister than average conditions (Garreaud et al., 2009). Beyond 60°S, negative anomalies of mean sea level pressure are noticed (Fogt & Marshall, 2020). Conversely, opposite anomalies are observed during the negative phase of SAM. Indeed, the effects mentioned above are partially reflected in the significant correlations with SAM and the Z300 Drake index ($r = -0.26*$) and the R2-SST index ($r = 0.35*$). Furthermore, the notable, positive, and significant correlation between PC1 and large-scale indices such as SAM, T850 Drake, and R2-SST ($r \geq 0.56*$) lead us to hypothesize that these variables are linked with the spatial pattern of the first mode, suggesting an increase in temperature not only at the surface but also in the troposphere, especially in northwest Patagonia.

The second mode explains 8% of the variability of H0 and is characterized by a meridional gradient, showing positive values in the northeast region and negative values in the southwest. The significant correlations that we found on this occasion are with the indices Z300 Drake ($r = -0.68*$), T850 Drake ($r = -0.51*$) and R3-U850 ($r = 0.53*$). On the other hand, the third mode represents around 4% of the variability of H0 and displays a zonal gradient with positive values in the northwestern side and negative values in the southeast. Significant correlation between pairs of indices and this mode only was found with Z300 Drake ($r = 0.39*$) and R3-U850 ($r = -0.41*$). Additionally, the correlation obtained from indices such as ENSO (NIÑO 1+2 and NIÑO 3.4) with the leading modes showed low and non-statistically significant correlations ($|r|<0.2$).
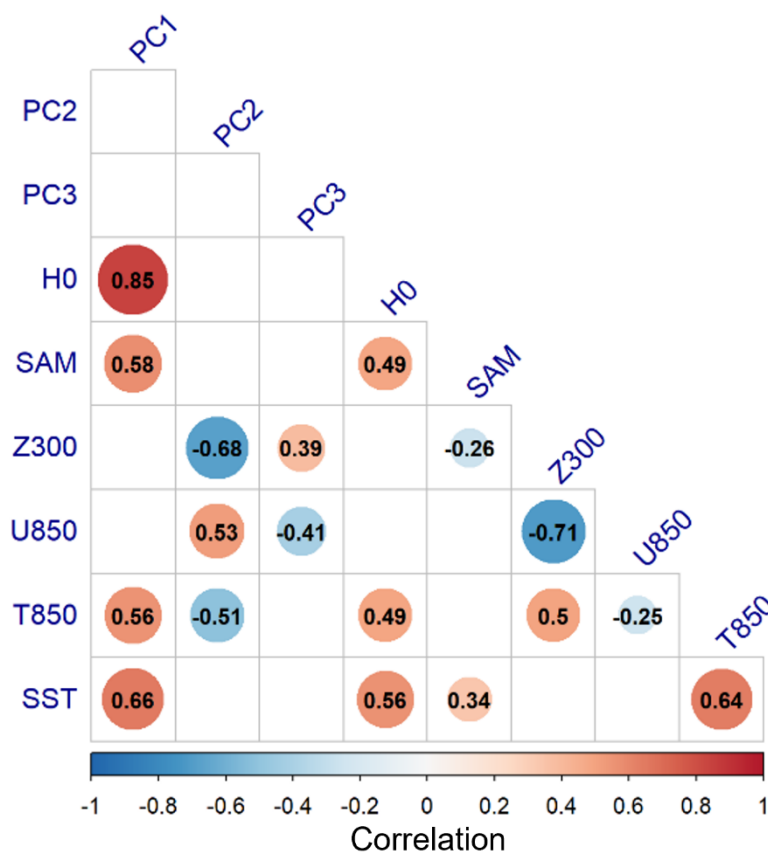
Figure 9: The correlation matrix between the standardized indices, H0 anomalies, and principal components obtained from the analysis is presented in the following. Only statistically significant values (p-value < 0.05) are shown.

3.6 Trends of H_0

As depicted in Figure 8a, the average height anomalies of the 0°C isotherm field are indeed increasing significantly compared to the historical record (1959-2021), with a marked and unprecedented trend in the period that began 2010. This increment is also consistent with the spatial and temporal pattern of the leading mode. To further investigate this phenomenon, we calculated the spatial distribution of H_0 trends in the area, focusing only on fields with significant trends. Figure 10 presents the summer field (DJF), as well as for autumn (MAM), winter (JJA), and spring (SON).

During summers, the most pronounced trends are estimated in comparison to other seasons ($\bar{H}_0^{Trend} = 40$ m/decade), particularly notable in the northwest region of Patagonia, where the core demonstrates significant average values reaching approximately 61 m/decade. During this season, the meridional gradient experiences its most abrupt variation, with an

330   amplitude of IQR of 58-19 m/decade between the northern (41°S) and southern areas (~50°S). Concerning the zonal gradient in this period, the west slope of the Andes retains its distinction for having the highest trends, in contrast to the east slope, where around of 72°W, the trends values becoming smaller. Furthermore, the higher amplitude of the zonal IQR is 68-18 m/decade, located in 73°W, thus indicating that around that longitude there is a wide variability in the estimated significant trends.

335

The trends diminish during autumns ($\overline{H}_0^{Trend} = 36$ m/decade), and there is a shift in the spatial distribution of these trends. Unlike the previous season, the field becomes more homogeneous, with the high values of trends spread in northwest and the middle area, and with a low intense meridional and zonal gradient. The amplitude of IQR of meridional and zonal profile spanning between 45-17 and 46-23 m/decade, respectively.

340

In winters, the trend continues to decrease reaching the second lowest seasonal value ($\overline{H}_0^{Trend} = 19$ m/decade). Our findings indicate that these lower trend values are primarily concentrated over the southern Andes (73.25°W, ~9 m/decade). Beyond this range, we observe an escalation in trends, with the highest values situated over the central eastern Patagonia (70.5°W, 17.5 m/decade). Consequently, the meridional gradient experiences variations compared to the autumn period with low
345   values, spanning between 31-10 m/decade. Concerning the zonal profile, the changes are relatively minor, resulting in an amplitude range of 30-9 m/decade.

Notably, the lowest trends are depicted in spring ($\overline{H}_0^{Trend} = 16$ m/decade). If we focus the distribution of trend values are homogeneous, therefore as well the meridional and zonal gradient is quite flat with little variations. Taking into consideration
350   the significant values, it is evident that this seasonal distribution is the most homogeneous, except for the northwestern and central Patagonia regions, where slight increases in the trend are observed (23 m/decade). As a result of this, the range of meridional and zonal amplitudes is smaller, ranging from 21-11 and 23-12 m/decade, respectively.
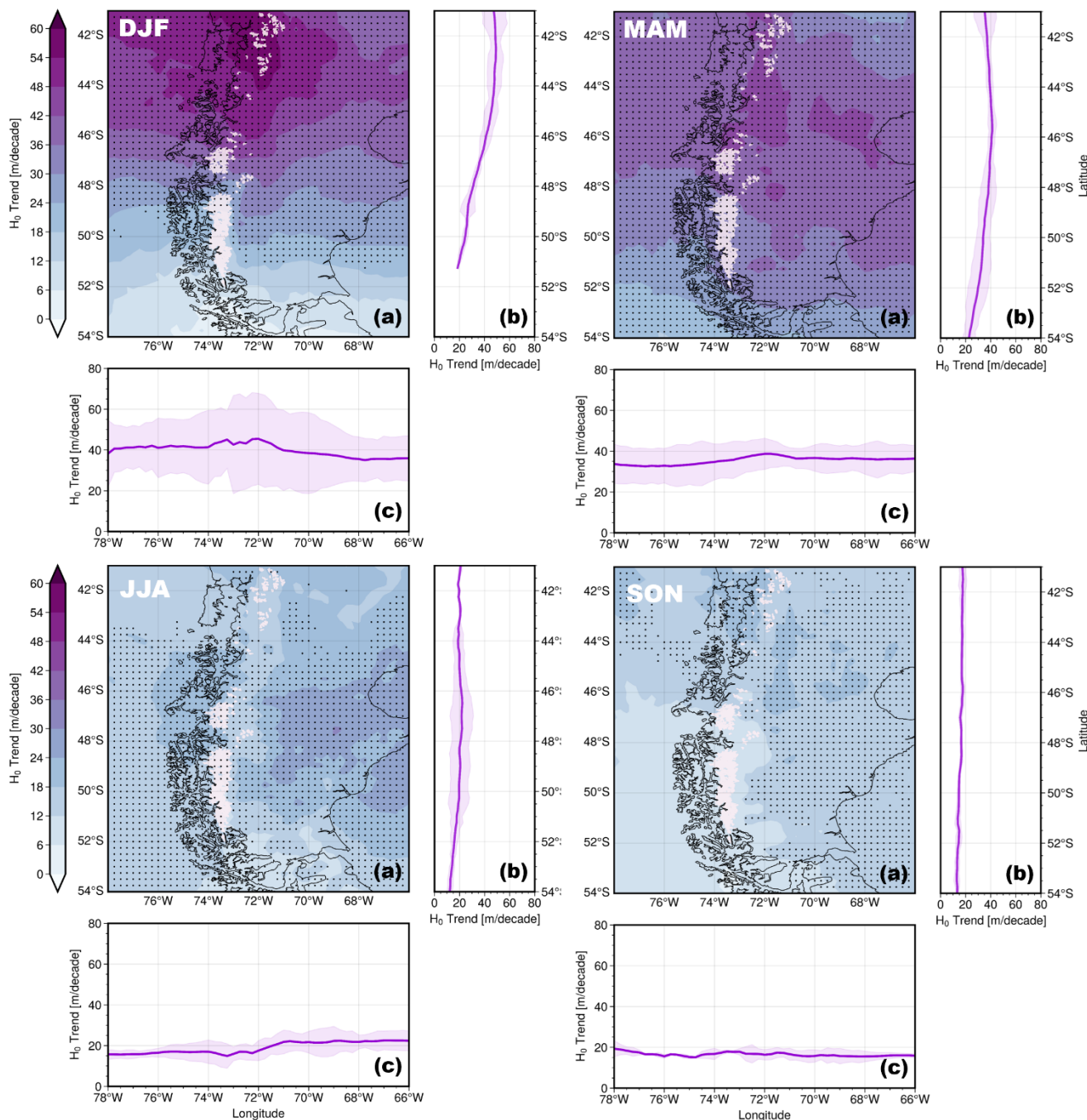
Figure 10: Spatial distribution of the 0°C isotherm trends (H0) across the year and seasons. Lighter areas depict a lower altitude of the trends, while purple areas indicate higher values. The white contours delineate the extent of ice coverage in the region. Each distribution is accompanied by a latitudinal profile (b) and a longitudinal profile (c), showcasing the spatially averaged H0 trend values. The purple shaded area in these profiles represents the interquartile range. Black circles denote statistically significant trends at p-value < 0.05.

360

4 Discussion

The validation process quantified the model's uncertainties regarding daily-scale measurements. However, our methodology did not reduce the number of observations through an analysis of observed data quality. Instead, it focused on using radiosonde temperature profiles with at least 3 observed data points to ensure a minimum number of observations for

365   determining a freezing level between layers. We chose to employ this methodology because the number of stations with data in the area was quite limited. Nevertheless, despite this constraint, the validation process results indicated a high similarity between the estimated freezing level from observed and modeled data.

At the Río Gallegos station, which had the most limitations due to the limited number of observations, the model showed the

370   greatest difference from the observations. This difference was primarily due to lowest correlation (in contrast with other stations; $r = 0.8*$) and higher RMSE (445 meters). Despite the limited data during the period, they yield indices that indicate a range of uncertainty in the unfavorable case scenario. Furthermore, it's worth noting that the RMSE is one of the metrics that penalizes differences between observed and simulated data the most.

375   In relation to uncertainty (RMSE), the daily-scale validation of the modeled field for the 0°C isotherm resulted in a range that varies between 240 and 445 meters. When considering monthly and decade-scale analyses, this corresponds to an RMSE value of 227 to 72 meters and 114 to 39 meters, respectively. As a result, certain estimated values (such as interquartile range and trends) lie within this range of uncertainties, and the obtained results are influenced by these uncertainties.

380   The spatial configuration of the 0°C isotherm data indicates clear differences between the north-south and east-west slopes of the Andes in our study area. This distribution implies that at the same latitude, lower isotherm values are found on the western side, while higher values are recorded towards the east. These characteristics are replicated at least down to 52°S, as this configuration is no longer observed at higher latitudes, coinciding with the gradual topographical descent of the AA. Furthermore, these results are consistent with (Garreaud et al., 2009) results, where the spatial arrangement of the annual

385   average temperature field at 925 hPa is depicted. This updated analysis using ERA5 data suggests a similar distribution (Figure S3), highlighting the strong influence of topography on tropospheric temperatures.

Following the established temperature distribution, a particularly noteworthy finding of our analysis emerges in the northwestern Patagonia. Here, both the first mode of the EOF (EOF1), strongly correlated with H0 anomalies, and the trend

390   field (both annual and summer) unveil a core characterized by elevated 0°C isotherm values. The observed correlations lead us to posit that this phenomenon is attributed to factors modulating regional temperatures, primarily influenced by the Pacific

Ocean's proximity to Patagonia's western coast and interannual variability mechanisms such as the Southern Annular Mode (SAM). This observation is remarkable, as it suggests SAM not only impacts surface temperature fluctuations but also extends its influence on tropospheric temperatures, which is a logical outcome given the tropospheric adiabatic warming

395 prevailing in the equatorial realm of the polar jet triggered by SAM in the area.

Moreover, a better perspective emerges as we delve into Figure S4a, unveiling the most pronounced correlations concentrated and spreading from 45°S-68°W (eastern Patagonia). This specific region aligns with one of the three key focal points of positive atmospheric pressure anomalies of SAM configuration global patterns. In terms of sea surface temperature,

400 Figure S4c affirms robust correlations spanning the entire area, accentuated by heightened values along the western coast.

However, concerning the Drake Passage, its involvement in the depicted configuration (EOF1) is not readily apparent, contrary to expectations given its dynamics (Carrasco-Escaff et al., 2023), which should ideally exhibit stronger correlations not only with local temperature but also with geopotential height (Z300) and wind patterns (R3-U850). Interestingly, the

405 situation alters with the configuration proposed by mode 2 (EOF2), where more compelling correlations emerge. This phenomenon might be linked to clear sky conditions and inversion layers, contributing to a reduction in the height of the 0°C isotherm. Notably, this aligns well with the freezing level algorithm's design, prioritizing the initial transition to 0°C within the atmosphere. In support of this notion, Figure S4b and S4d exhibit anomalous high-pressure centers near the Drake Passage that induce strong, positive correlations with freezing level heights, particularly evident in southwestern Patagonia.

410

Lastly, the third mode (EOF3) sustains significant correlations, potentially indicative of atmospheric conditions associated with pronounced migration patterns and consequent Foehn events. This interpretation gains support from Figure 13f, which reveals noteworthy negative correlations concentrated along the western slopes of the Andes.

415 Our study underscores the upward shift in the 0°C isotherm's elevation within the region over the study period, potentially affecting water resources due to the reduction in glacier volumes. This significance is magnified by the region's vulnerability to natural hazards like floods and GLOFs. In line with this, (Bravo et al., 2019) determined that augmented snow accumulation primarily stems from local topography, confined to the regional level with elevated snow deposition beyond 1,000 meters along the western perimeters of the icefields. Consequently, in a scenario where these conditions persist or

420 aggravate, our projections indicate impending changes that could result in diminished snow accumulation, increased ice exposure, and intensified melting at this height.

5 Conclusions

Through vertical temperature profiles, values of the 0°C isotherm height were obtained using radiosonde observations and ERA5 data from 1959-2021 in Patagonia. The modeled data used showed robust estimation of daily observed values and

425 facilitated the derivation of spatial averages that describe the state of the 0°C isotherm within the study area. Employing correlations, the relationship between the main atmospheric modes of 0°C isotherm interannual variability and time series of different climatic indices was investigated. This approach aimed to discern the large-scale climatic processes governing interannual variations of the freezing level in Patagonia. Some significant findings are:

430 The histogram of spatial averages reveals that isotherms in the western Andes zone (western section of 72°W) have an average (median) around 1568 (1347) m.a.s.l. In contrast, the eastern Andes zone shows a higher mean (median) of 1818 (1709) m.a.s.l. Overall, the mean (median) freezing level for the entire region lies around 1691 (1519) m.a.s.l.

Seasonal variations indicate that the 0°C isotherm's amplitude spans heights ranging from 3480 to 585 m.a.s.l. The lowest

435 height is estimated during winter months, while the highest occurs in summer.

A pronounced zonal gradient is noteworthy, intensifying around 72°W, associated with a drier atmosphere influenced by the topographic effect of the Andes. The meridional gradient behaves as expected (typical temperature gradient of the transition to extratropic), gradually decreasing with latitude. This spatial configuration persists throughout the months, with the

440 distinction that higher freezing level heights are recorded during summers. In this season, the zonal average is estimated not to intersect with the highest topography (95th percentile of topography). Contrasting conditions prevail during winter, where the lowest freezing level values are observed, and on average, the zonal profile of the 0°C isotherm intersects the highest (P95) and lowest (P5) topography around 72°W, essentially aligning with the Andes Mountain range. Autumn and spring months act as transitional periods between the more pronounced summer and winter seasons.

445

The primary mode of variability accounts for about 84% of the variance in the H0 field. Spatially, this mode indicates positive values across the entire area, particularly in central and northeastern Patagonia. Temporally, this mode shares much of the interannual variability with the average field of 0°C isotherm anomalies in Patagonia. Thus, years with positive phases of the first principal component (PC1) are associated with positive anomalies in freezing level height. Similarly, this mode

450 shows a positive and significant correlation with SAM, temperature at 850 hPa in the Drake Passage, and sea surface temperature in the Pacific Ocean near the western coasts of Patagonia. The second and third modes explain 8% and 4.4% of the data variance, respectively. Their spatial configuration indicates both a meridional and zonal dipole in the study area. The second mode exhibited significant correlations with R1-Z300 (+), R1-T850 (-), and R3-U850 (-). Meanwhile, the third mode showed significant correlations with R1-300 (+) and R3-U850 (-).

455

In a broad sense, throughout the seasons, the 0°C isotherm level exhibited a consistent variation with temperature changes, marked by an increase in temperature within the whole region. The highest trends were obtained during summers, specifically in northwestern Patagonia, around the Andes, indicating an average increase in freezing level heights of 61 m/decade. In average, winter trends are lower but remain positive, reaching average values of 8 m/decade in areas 460 surrounding the Andes.

Code availability

Preprocessing script along with the corresponding files are available at 10.5281/zenodo.10493785

Data availability

465 ERA5 pressure levels (Hersbach et al., 2023) was acquired from the Copernicus climate data store.

Author contributions

All authors participated in the conceptualization and methodology of the research. CB and AGR proposed the research topic. NG and PM carried out the software development, data curation and analysis. NG was in charge of project administration, resources, validation, visualization and draft writing. All authors contributed to the review and editing of the manuscript.

470 ## Acknowledgments

References

475 Abram, N. J., Mulvaney, R., Vimeux, F., Phipps, S. J., Turner, J., & England, M. H. (2014). Evolution of the Southern Annular Mode during the past millennium. Nature Climate Change 2014 4:7, 4(7), 564–569. https://doi.org/10.1038/nclimate2235

Aravena, J. C., & Luckman, B. H. (2009). Spatio-temporal rainfall patterns in Southern South America. International Journal of Climatology, 29(14), 2106–2120. https://doi.org/10.1002/JOC.1761

480 Bravo, C., Bozkurt, D., Gonzalez-Reyes, Á., Quincey, D. J., Ross, A. N., Farías-Barahona, D., & Rojas, M. (2019). Assessing snow accumulation patterns and changes on the Patagonian Icefields. Frontiers in Environmental Science, 7(MAR). https://doi.org/10.3389/fenvs.2019.00030

Bravo, C., Ross, A. N., Quincey, D. J., Cisternas, S., & Rivera, A. (2021). Surface ablation and its drivers along a west-east transect of the Southern Patagonia Icefield. https://doi.org/10.1017/jog.2021.92

485 Carrasco-Escaff, T., Rojas, M., Garreaud, R. D., Bozkurt, D., & Schaefer, M. (2023). Climatic control of the surface mass balance of the Patagonian Icefields. Cryosphere, 17(3), 1127–1149. https://doi.org/10.5194/tc-17-1127-2023

Durre, I., Yin, X., Vose, R. S., Applequist, S., & Arnfield, J. (2018). Enhancing the data coverage in the integrated Global Radiosonde Archive. Journal of Atmospheric and Oceanic Technology, 35(9), 1753–1770. https://doi.org/10.1175/JTECH-D-17-0223.1

490 Dussaillant J., A., Buytaert, W., Meier, C., & Espinoza, F. (2012). Hydrological regime of remote catchments with extreme gradients under accelerated change: the Baker basin in Patagonia. Hydrological Sciences Journal, 57(8). https://doi.org/10.1080/02626667.2012.726993

Fogt, R. L., & Marshall, G. J. (2020). The Southern Annular Mode: Variability, trends, and climate impacts across the Southern Hemisphere. In Wiley Interdisciplinary Reviews: Climate Change (Vol. 11, Issue 4). Wiley-Blackwell.
495 https://doi.org/10.1002/wcc.652

Garreaud, R. D., Vuille, M., Compagnucci, R., & Marengo, J. (2009). Present-day South American climate. Palaeogeography, Palaeoclimatology, Palaeoecology, 281(3–4), 180–195. https://doi.org/10.1016/j.palaeo.2007.10.032

Garreaud, R., Lopez, P., Minvielle, M., & Rojas, M. (2013). Large-scale control on the Patagonian climate. Journal of Climate, 26(1), 215–230. https://doi.org/10.1175/JCLI-D-12-00001.1

500 Hersbach, H., Bell, B., Berrisford, P., Hirahara, S., Horányi, A., Muñoz-Sabater, J., Nicolas, J., Peubey, C., Radu, R., Schepers, D., Simmons, A., Soci, C., Abdalla, S., Abellan, X., Balsamo, G., Bechtold, P., Biavati, G., Bidlot, J., Bonavita, M., … Thépaut, J. N. (2020). The ERA5 global reanalysis. Quarterly Journal of the Royal Meteorological Society, 146(730), 1999–2049. https://doi.org/10.1002/qj.3803

Hugonnet, R., McNabb, R., Berthier, E., Menounos, B., Nuth, C., Girod, L., Farinotti, D., Huss, M., Dussaillant, I., Brun, F.,
505 & Kääb, A. (2021). Accelerated global glacier mass loss in the early twenty-first century. Nature 2021 592:7856, 592(7856), 726–731. https://doi.org/10.1038/s41586-021-03436-z

Iribarren Anacona, P., Mackintosh, A., & Norton, K. P. (2015). Hazardous processes and events from glacier and permafrost areas: lessons from the Chilean and Argentinean Andes. Earth Surface Processes and Landforms, 40(1), 2–21. https://doi.org/10.1002/ESP.3524

510 Lenaerts, J. T. M., Van Den Broeke, M. R., Van Wessem, J. M., Van De Berg, W. J., Van Meijgaard, E., Van Ulft, L. H., & Schaefer, M. (2014). Extreme Precipitation and Climate Gradients in Patagonia Revealed by High-Resolution Regional Atmospheric Climate Modeling. Journal of Climate, 27(12), 4607–4621. https://doi.org/10.1175/JCLI-D-13-00579.1

Malz, P., Meier, W., Casassa, G., Jaña, R., Skvarca, P., & Braun, M. H. (2018). Elevation and mass changes of the southern Patagonia icefield derived from TanDEM-X and SRTM data. Remote Sensing, 10(2). https://doi.org/10.3390/rs10020188

515 Mardones, P., & Garreaud, R. D. (2020). Future changes in the free tropospheric freezing level and rain–snow limit: The case of central Chile. Atmosphere, 11(11), 1–16. https://doi.org/10.3390/atmos11111259

Masiokas, M. H., Rabatel, A., Rivera, A., Ruiz, L., Pitte, P., Ceballos, J. L., Barcaza, G., Soruco, A., Bown, F., Berthier, E., Dussaillant, I., & MacDonell, S. (2020). A Review of the Current State and Recent Changes of the Andean Cryosphere. Frontiers in Earth Science, 8, 503838. https://doi.org/10.3389/FEART.2020.00099/BIBTEX

520 Minowa, M., Schaefer, M., Sugiyama, S., Sakakibara, D., & Skvarca, P. (2021). Frontal ablation and mass loss of the Patagonian icefields. Earth and Planetary Science Letters, 561. https://doi.org/10.1016/j.epsl.2021.116811

North, G. R., Bell, T. L., Cahalan, R. F., & Moeng, F. J. (1982). Sampling Errors in the Estimation of Empirical Orthogonal Functions. Monthly Weather Review, 110(7). https://doi.org/10.1175/1520-0493(1982)110<0699:seiteo>2.0.co;2

Roe, G. H. (2004). OROGRAPHIC PRECIPITATION. Https://Doi.Org/10.1146/Annurev.Earth.33.092203.122541, 33, 525 645–671. https://doi.org/10.1146/ANNUREV.EARTH.33.092203.122541

Sauter, T. (2020). Revisiting extreme precipitation amounts over southern South America and implications for the Patagonian Icefields. Hydrology and Earth System Sciences, 24(4), 2003–2016. https://doi.org/10.5194/HESS-24-2003-2020

Schauwecker, S., Rohrer, M., Huggel, C., Endries, J., Montoya, N., Neukom, R., Perry, B., Salzmann, N., Schwarb, M., & Suarez, W. (2017). The freezing level in the tropical Andes, Peru: An indicator for present and future glacier extents. Journal 530 of Geophysical Research: Atmospheres, 122(10), 5172–5189. https://doi.org/10.1002/2016JD025943

Siler, N., Roe, G., & Durran, D. (2013). On the Dynamical Causes of Variability in the Rain-Shadow Effect: A Case Study of the Washington Cascades. Journal of Hydrometeorology, 14(1), 122–139. https://doi.org/10.1175/JHM-D-12-045.1

Somos-Valenzuela, M. A., Oyarzun-Ulloa, J. E., Fustos-Toribio, I. J., Garrido-Urzua, N., & Chen, N. (2020). The mudflow disaster at Villa Santa Lucía in Chilean Patagonia: Understandings and insights derived from numerical simulation and 535 postevent field surveys. Natural Hazards and Earth System Sciences, 20(8), 2319–2333. https://doi.org/10.5194/NHESS-20-2319-2020

van der Geest, K., & van den Berg, R. (2021). Slow-onset events: a review of the evidence from the IPCC Special Reports on Land, Oceans and Cryosphere. Current Opinion in Environmental Sustainability, 50, 109–120. https://doi.org/10.1016/J.COSUST.2021.03.008

540 Viale, M., & Garreaud, R. (2014). Summer Precipitation Events over the Western Slope of the Subtropical Andes. Monthly Weather Review, 142(3), 1074–1092. https://doi.org/10.1175/MWR-D-13-00259.1

Wilks, D. S. (2019). Statistical Methods in the Atmospheric Sciences, Fourth Edition. In Statistical Methods in the Atmospheric Sciences, Fourth Edition. https://doi.org/10.1016/C2017-0-03921-6.